

## Environmental Research Letters



## LETTER

## On the observed hysteresis in field-scale soil moisture variability and its physical controls

## OPEN ACCESS

## RECEIVED

13 March 2016

## REVISED

5 July 2016

## ACCEPTED FOR PUBLICATION

20 July 2016

## PUBLISHED

5 August 2016

Original content from this work may be used under the terms of the [Creative Commons Attribution 3.0 licence](https://creativecommons.org/licenses/by/3.0/).

Any further distribution of this work must maintain attribution to the author(s) and the title of the work, journal citation and DOI.

G Mascaro<sup>1,2</sup> and E R Vivoni<sup>1,3</sup><sup>1</sup> School of Sustainable Engineering and the Built Environment, Arizona State University, Tempe, 126b, 21 E 6th St, Tempe, AZ 85281, USA<sup>2</sup> Julie Ann Wrigley Global Institute of Sustainability, Arizona State University, Tempe, 126b, 21 E 6th St, Tempe, AZ 85281, USA<sup>3</sup> School of Earth and Space Exploration, Arizona State University, Tempe, 126b, 21 E 6th St, Tempe, AZ 85281, USAE-mail: [gmascaro@asu.edu](mailto:gmascaro@asu.edu)**Keywords:** soil moisture field experiment, spatial variability, North American monsoon, semiarid ecosystems, land surface hydrologySupplementary material for this article is available [online](#)**Abstract**

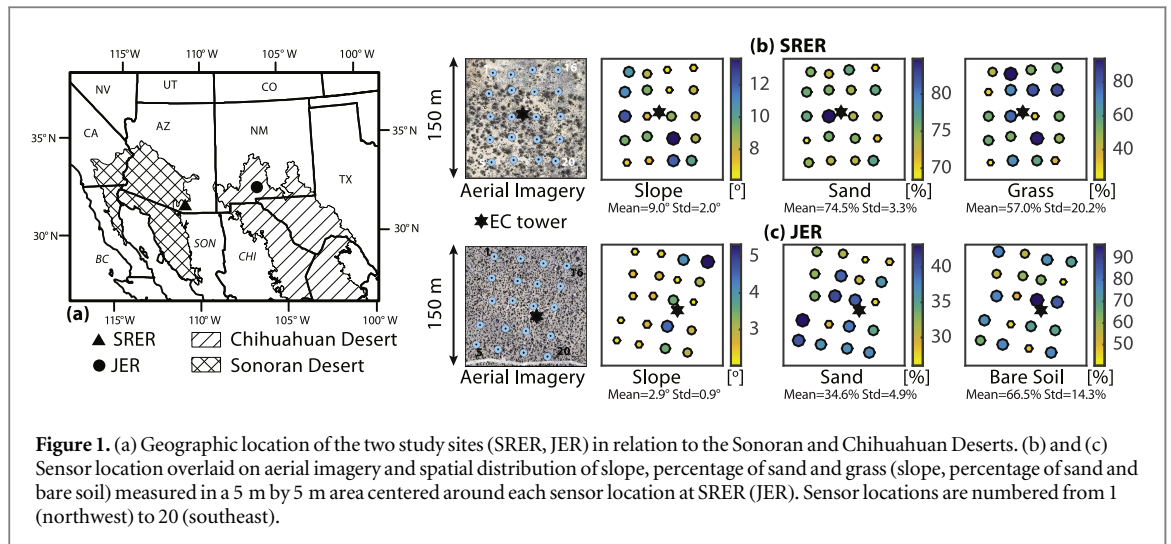
The spatiotemporal variability of soil moisture ( $\theta$ ) has rarely been studied at the field scale across different seasons and sites. Here, we utilized 9 months of  $\theta$  data in two semiarid ecosystems of North America to investigate the key relationship between the spatial mean ( $\langle\theta\rangle$ ) and standard deviation ( $\sigma_\theta$ ) at the field-scale ( $\sim 100$  m). Analyses revealed a strong seasonal control on the  $\sigma_\theta$  versus  $\langle\theta\rangle$  relation and the existence of hysteretic cycles where wetting and dry-down phases have notably different behavior. Empirical orthogonal functions (EOFs) showed that  $\theta$  variability depends on two dominant spatial patterns, with time-stable and seasonally varying contributions in time, respectively. Correlations between EOFs and land surface properties also indicated that  $\theta$  patterns are linked to vegetation (terrain and soil) factors at the site with higher (lower) vegetation cover. These physical controls explained the observed hysteresis cycles, thus confirming interpretations from previous modeling studies for the first time.

**1. Introduction**

Soil moisture ( $\theta$ ) is a critical state variable controlling the feedback between the water, energy and carbon cycles (Entekhabi 1995). As a result, quantifying its spatiotemporal variability and identifying its associated physical controls at different scales is crucial for diagnostic and prognostic studies in the areas of hydrology, climate, atmospheric science, ecology, and agronomy, among others (Tao *et al* 2003, Entekhabi *et al* 2010, Seneviratne *et al* 2010, Mascaro and Vivoni 2012, Dillon *et al* 2016). A simple way to characterize the spatiotemporal variability of  $\theta$  is through the relation between its spatial mean ( $\langle\theta\rangle$ ) and variability (measured by the standard deviation,  $\sigma_\theta$ , or the coefficient of variation,  $CV = \sigma_\theta/\langle\theta\rangle$ ). This relation has been investigated using observations and models over different spatial extents, ranging from field ( $\sim 100$  m) to regional ( $> 100$  km) scales, and diverse settings (e.g., Famiglietti *et al* 2008, Brocca *et al* 2010, Li and Rodell 2013). Previous studies have shown that the  $\sigma_\theta$  versus  $\langle\theta\rangle$  relation has an upward

convex shape independently of the spatial extent, while the range of  $\langle\theta\rangle$  depends on local climate. Moreover, Rosenbaum *et al* (2012) recently showed the presence of hysteretic cycles in the relation by analyzing one year of  $\theta$  data collected in a humid basin of 0.27 km<sup>2</sup> in Germany. Prior to this study, the occurrence of hysteretic patterns was only identified and discussed through modeling experiments (Ivanov *et al* 2010, Vivoni *et al* 2010, Fatichi *et al* 2015, Ji *et al* 2015).

While the general shape of the  $\sigma_\theta$  versus  $\langle\theta\rangle$  relation is explained by the bounded nature of  $\theta$ , the physical factors (climate, vegetation, soil and topography) controlling the range of  $\sigma_\theta$  values observed for the same  $\langle\theta\rangle$ , the possible existence of hysteresis, and the shape of the relation within different  $\langle\theta\rangle$  intervals are not fully understood (Vanderlinden *et al* 2012). A number of hypotheses have been formulated to explain the controls on these patterns based on synthetic numerical experiments, which highlighted the greater importance of vegetation (soil) properties in temperate and semiarid (humid) climates, where  $\langle\theta\rangle$



tends to be low (high) (e.g., Lawrence and Hornberger 2007, Fatichi *et al* 2015). However, the validation of these hypotheses has been prevented by the lack of high-resolution soil moisture observations, such as those provided by dense automated networks. This is especially true in semiarid areas, where distributed measurements would be required to capture the high spatial heterogeneity of soil and vegetation properties (Ochsner *et al* 2013).

We address this gap by conducting a comparative study in two semiarid ecosystems that are representative of the Sonoran and Chihuahuan Deserts (~622 000 km<sup>2</sup> in North America). Both sites have transitioned from grasslands to shrublands as a consequence of woody plant encroachment (Van Auken 2000). Regional climate is characterized by a marked seasonality due to North American monsoon occurring from July to September, which accounts for 40%–70% of the annual precipitation (Adams and Comrie 1997) and leads to the greening of drought-deciduous plants. Numerical studies have shown that the seasonal variation of climatic forcings and vegetation lead to complex soil moisture dynamics, with possible hysteretic patterns in the  $\sigma_\theta$  versus  $\langle\theta\rangle$  relation and whose physical controls change in time (e.g., Vivoni *et al* 2010, Yetemen *et al* 2015). Here, we use direct observations over a 9 month period from dense sensor networks installed at the two sites to: (i) investigate the field-scale spatiotemporal variability of  $\theta$ , its seasonality in the  $\sigma_\theta$  versus  $\langle\theta\rangle$  space, and the occurrence of hysteresis; and (ii) identify the associated physical controls in the two ecosystems by means of an empirical orthogonal function (EOF) analysis.

## 2. Study area and datasets

The two study sites are located in the Santa Rita (SRER) and Jornada (JER) experimental ranges in southern Arizona and New Mexico, respectively (figure 1(a)). Climate at SRER is characterized by hotter conditions

than JER (mean annual temperature of 22 °C and 18 °C, respectively), mostly because of differences in elevation (1170 and 1470 m). SRER also receives a larger mean annual precipitation than JER (370 and 280 mm, respectively). As a consequence of these differences, vegetation is characterized as a woody savanna at SRER and a mixed shrubland at JER. Recently, an eddy covariance (EC) tower was installed at each site to measure hydrometeorological variables and surface turbulent fluxes, along with a distributed sampling network to capture the spatial variability of  $\theta$  around the tower. The networks have a similar design consisting of twenty locations distributed over a five-by-four grid (~150 m by 120 m) with a regular spacing of ~30 m and sensors at two depths (5 and 15 cm). Details on the instrument networks are provided by Anderson and Vivoni (2016).

Here, we use observations of  $\theta$ , as well as precipitation (P) and evapotranspiration (ET), from 1 July 2013 to 31 March 2014 at 30 min resolution. Soil moisture data were averaged over the two sensor depths, thus representing the first 20 cm of soil. Missing  $\theta$  data were reconstructed through temporal interpolation for gaps smaller than 12 h or by averaging concurrent data of the five neighboring locations with high correlations (always >0.84). To characterize local terrain, soil and vegetation, we computed the following factors in a 5 m by 5 m area centered on each sensor location: mean slope and curvature, derived from aerial imagery at 1 m resolution; percentage of gravel, sand, silt and clay obtained from soil samples collected at comparable depths; and percentage of the vegetation classes through the analysis of orthoimages at 50 cm resolution (grass, prickly pear, mesquite and bare soil at SRER; bare soil, grass, mesquite, creosote and other shrubs at JER) (Anderson and Vivoni 2016). As shown in figures 1(b) and (c), SRER is mostly characterized by sandy soil and grass vegetation, while JER is mainly bare soils with sand and gravel textures. More complete information on the land surface factors is

reported in figures S1 and S2. Finally, 16-day composites of the normalized difference vegetation index (NDVI) from the moderate resolution imaging spectroradiometer (MODIS) were acquired in the two 250 m by 250 m pixels containing each network to quantify vegetation greening.

### 3. Methods

We investigated the relation between  $\sigma_\theta$  and  $\langle\theta\rangle$  by (i) dividing the study period into summer (July–September, 2013), fall (October–December, 2013), and winter (January–March, 2014) periods, with the aim of exploring differences due to the seasonality; and (ii) tracking the time evolution of the relation to identify the occurrence of hysteretic cycles. To identify the physical controls on the spatiotemporal variability, we conducted an EOF analysis (Hannachi *et al* 2007). This technique decomposes a space-time dataset into time-invariant orthogonal spatial patterns (the EOFs) and corresponding space-invariant time series of coefficients (the principal components, PCs) that control the importance of each EOF in time. The EOF analysis has been previously applied at catchment and regional scales using  $\theta$  fields from instrument networks collected on a limited number of dates (up to 15 d) (e.g., Korres *et al* 2010, Busch *et al* 2012). Here, we focus on a smaller spatial extent (field scale) that has received much less attention (Vereecken *et al* 2014) and, for the first time, we use seasonally varying  $\theta$  data covering a wider range of wetness conditions and climate forcing.

The EOF technique was applied as follows: (i) for each time step, we computed the spatial anomalies by subtracting the spatial mean from  $\theta$  values observed at each location; (ii) we calculated eigenvalues and eigenvectors (the PCs) of the covariance matrix of the spatial anomalies; (iii) we projected the original anomaly dataset into the new space defined by the eigenvectors, obtaining the EOFs; and (iv) we identified the EOFs that explain most of the spatial variability and verified their statistical significance through the Kaiser's rule (Wilks 2006). Next, we provided a physical interpretation of the dominant EOFs by computing the correlation coefficients (CCs) between each EOF and the land surface factors previously defined. Finally, to explore how the importance of the EOFs (and the associated physical controls) varies in time, we calculated the percentage of the spatial variance explained by each EOF at each time step. For the  $k$ th EOF and  $j$ th time step, this is computed as:

$$PV_{k,j} = \frac{\sigma_{f,k}^2 e_{jk}^2}{\sigma_{\theta,j}^2} \cdot 100, \quad (1)$$

where  $\sigma_{\theta,j}^2$  is the spatial variance of the soil moisture network at time  $j$ ;  $\sigma_{f,k}^2$  is the spatial variance of the  $k$ th EOF; and  $e_{jk}$  is the PC of the  $k$ th EOF at time  $j$ . The derivation of equation (1) is described in text S1 in the

supporting information. Additional mathematical details on the EOF analysis applied to  $\theta$  fields are available in Jawson and Niemann (2007).

## 4. Results and discussion

### 4.1. Seasonality and Hysteresis in the relations between $\sigma_\theta$ and $\langle\theta\rangle$

Figures 2(a) and (d) present the seasonal relations between  $\sigma_\theta$  and  $\langle\theta\rangle$  at the two sites. To reduce noise,  $\theta$  data at 30 min resolution have been aggregated at the daily scale. We first analyzed the overall behavior by fitting all points to the analytical equation of Famiglietti *et al* (2008). The general shape of the relations ('Overall Fit') is upward convex at SRER and asymptotically increasing at JER. Nevertheless, a closer inspection reveals the importance of seasonality in establishing the general shape at each site. In summer, a large number of storm events ( $N$ ) and high values of ET lead to a large range of  $\langle\theta\rangle$ , and a greater scatter in  $\sigma_\theta$ , as compared to fall and winter seasons (detailed values of  $N$ ,  $P$  and  $ET$  are reported in table S1 of the supporting information). During the study period, the convex upward relation at SRER is caused primarily by a subset of fall and winter days with relatively high  $\langle\theta\rangle$  and low  $\sigma_\theta$ , whereas JER exhibits an asymptotic increase due to large number of summer days with high  $\langle\theta\rangle$  and high  $\sigma_\theta$ . These differences can be attributed to the high  $P$  at SRER (JER) during the fall (summer) season, exceeding the 75th (90th) percentile of the long-term records (table S1). This analysis reveals that using overall (single) relations obscures the superposition of complex spatial patterns that vary substantially across different seasons.

We further explored the  $\theta$  spatiotemporal variability by tracking the time-evolution of the  $\sigma_\theta$  versus  $\langle\theta\rangle$  relations. In both networks and for each season, we identified the occurrence of consecutive hysteretic cycles. Specifically, we found six (seven) cycles at SRER (JER), with three (four) in summer, one (one) in a transition between summer and fall, and two (two) in the fall and winter (lumped as fall/winter). Figure 2 presents examples of the observed hysteresis in summer (b), (e) and fall/winter (c), (f) seasons for each site, with all hysteretic cycles reported in figures S3 and S4. Following Ji *et al* (2015), we identified three phases in each hysteretic cycle: (i) a wetting phase with sharp increases in  $\langle\theta\rangle$  and  $\sigma_\theta$  due to precipitation; (ii) a redistribution phase prompted by a precipitation hiatus of 2–5 d followed by a short sequence of storm/inter-storm periods; and (iii) a dry-down phase with gradual decreases in  $\langle\theta\rangle$  and  $\sigma_\theta$  due to ET. For all hysteretic cycles, we computed statistics of their duration ( $D$ ), average  $P$  and  $ET$ , and the change in  $\langle\theta\rangle$  ( $\Delta\langle\theta\rangle$ ) and  $\sigma_\theta$  ( $\Delta\sigma_\theta$ , table S2). While a large diversity of hysteretic cycles is observed, shorter durations occur in summer (~15–17 d) as compared to fall/winter (~65–68 d) at

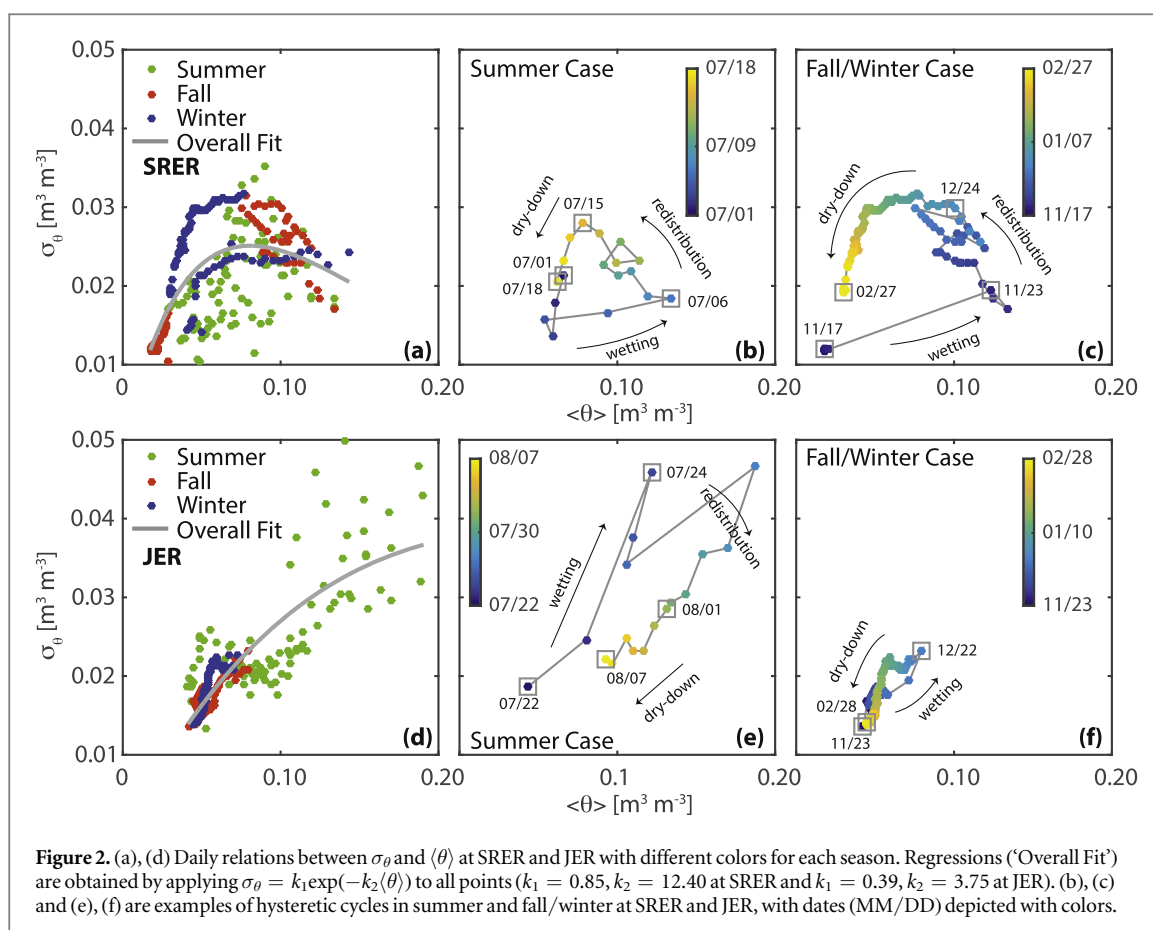


**Figure 2.** (a), (d) Daily relations between  $\sigma_\theta$  and  $\langle\theta\rangle$  at SRER and JER with different colors for each season. Regressions ('Overall Fit') are obtained by applying  $\sigma_\theta = k_1 \exp(-k_2 \langle\theta\rangle)$  to all points ( $k_1 = 0.85, k_2 = 12.40$  at SRER and  $k_1 = 0.39, k_2 = 3.75$  at JER). (b), (c) and (e), (f) are examples of hysteretic cycles in summer and fall/winter at SRER and JER, with dates (MM/DD) depicted with colors.

**Table 1.** Percentage of variance explained by two EOFs along with correlation coefficients to the main land surface factors. Bold indicates cases where the correlation is significant at 90% level ( $p$ -value < 0.1).

Percent	Correlation coefficient with land surface factors		
	Vegetation	Topography	Soil texture
SRER			
EOF1	76%	<b>-0.46 with % mesquite</b>	-0.39 with slope
EOF2	7%	-0.38 with % bare soil	0.36 with curvature
JER			
EOF1	53%	-0.39 with % creosote	<b>-0.62 with slope</b>
EOF2	29%	0.43 with % other shrubs	-0.35 with slope
			<b>-0.57 with % sand</b>
			<b>-0.47 with % clay</b>

both sites. This is due to a large (small) number of storms and high (low) ET rates in summer (fall/winter) and their respective quick (slow) wetting and dry-down phases. Wetting phases usually induce positive  $\Delta\langle\theta\rangle$  and  $\Delta\sigma_\theta$ , while dry-down phases have the opposite effect, thus closing the hysteretic cycles. Both clockwise and counterclockwise rotations are possible, depending on the spatiotemporal dynamics during redistribution phases. The redistribution (wetting) phase induces the largest changes in spatial variability ( $\Delta\sigma_\theta$ ) at SRER (JER), related to the sequence of storm/interstorm periods. These different pathways indicate that spatial variations during wetting and dry-down are affected in varying ways by land surface factors, as explored next.

#### 4.2. EOF analyses of $\theta$ and links to land surface factors

EOF analyses were applied on daily  $\theta$  observations at 14 locations at each site with greater than 50% of non-missing data. The first two EOFs (EOF1 and EOF2, figure S5) were found to be statistically significant (text S2) and together explain more than 80% of the variability of both datasets (table 1). As expected, EOF1 matches the spatial pattern of the time-averaged  $\theta$  (figure S6), while EOF2 resembles the pattern of the time standard deviation of  $\theta$  (the CCs are reported in table S3). Similar EOFs were also obtained with 30 min data, indicating that diurnal variations do not affect the dominant patterns. At SRER, EOF1 (76% of the explained variance) is primarily correlated with the

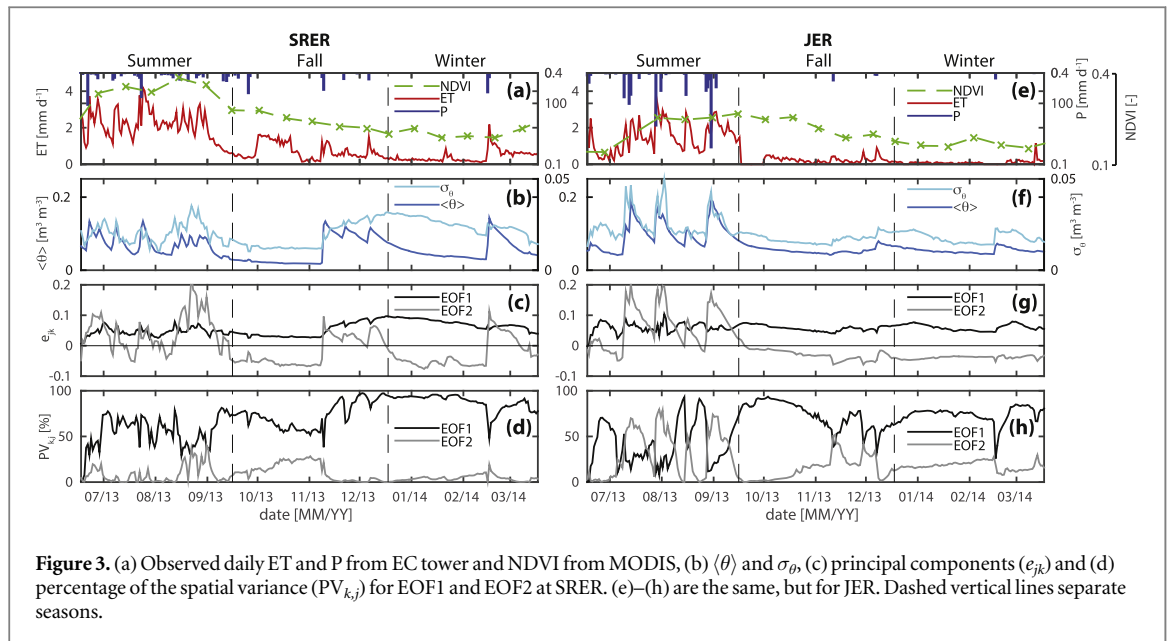


**Figure 3.** (a) Observed daily ET and P from EC tower and NDVI from MODIS, (b)  $\langle \theta \rangle$  and  $\sigma_\theta$ , (c) principal components ( $e_{jk}$ ) and (d) percentage of the spatial variance ( $PV_{k,j}$ ) for EOF1 and EOF2 at SRER. (e)–(h) are the same, but for JER. Dashed vertical lines separate seasons.

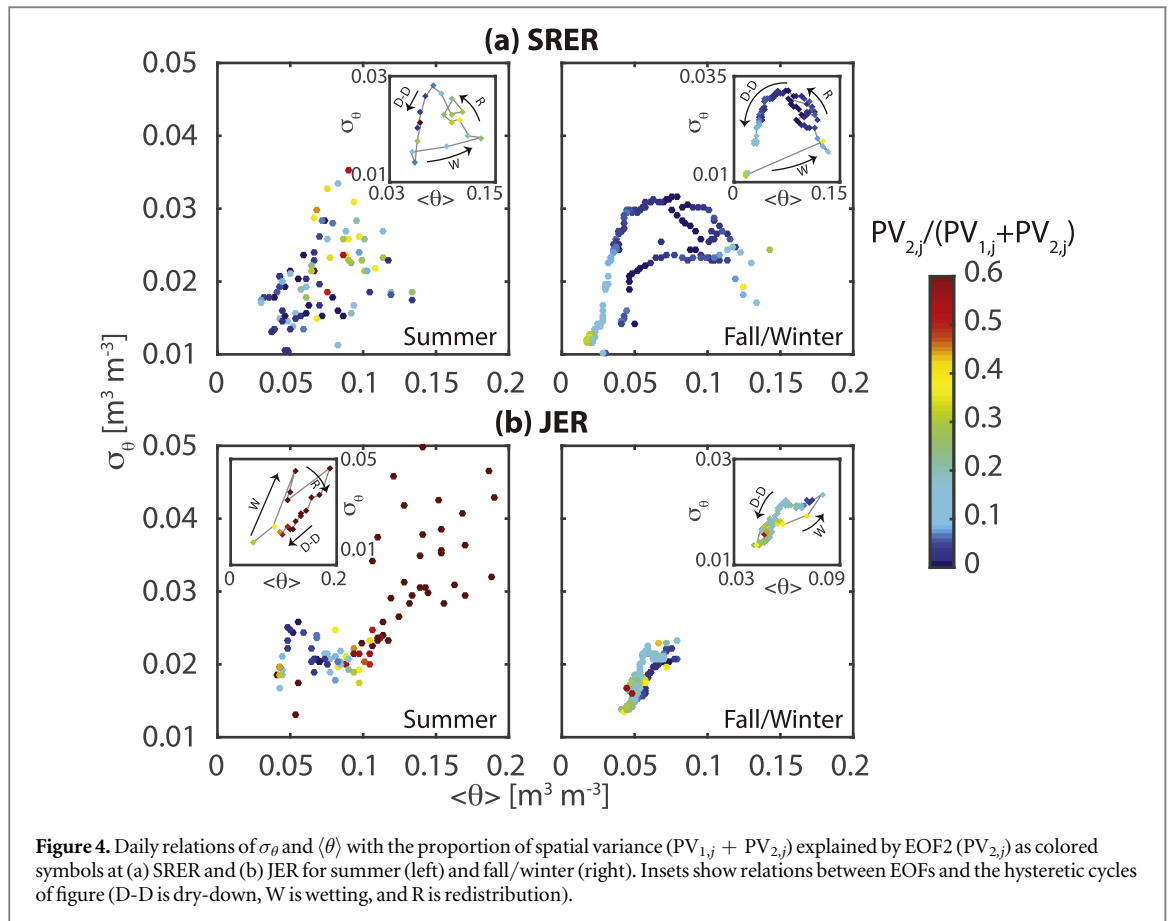
percentage of mesquite cover, while EOF2 (7%) does not have a statistically significant correlation with any factors. At JER, EOF1 (53%) is controlled by slope and sand content, while EOF2 (29%) is related to clay content. Table S3 details the correlation of land surface factors and the first two EOFs, including statistical significance ( $p$ -value) of the dominant factors. From the EOF analysis, it is clear that the spatiotemporal variability of  $\theta$  is controlled by a mixture of vegetation, soil and terrain factors, which together indicate local effects at the field scale (Grayson *et al* 1997). Correlations to land surface factors vary across the two sites, with the more (less) vegetated SRER (JER) exhibiting suppression (enhancement) of soil textural and terrain effects. These results are consistent with previous studies in other semiarid regions (e.g., Gómez-Plaza *et al* 2001) and differ from those in humid areas where both soil properties and subsurface lateral transport have a larger importance (e.g., Rosenbaum *et al* 2012).

Associated with the EOFs are PCs ( $e_{j1}$  and  $e_{j2}$ ) and their percentage of spatial variance explained ( $PV_{1,j}$  and  $PV_{2,j}$ ). Figure 3 relates these to time series of climatic forcings (P and ET), vegetation greenness (NDVI),  $\langle \theta \rangle$  and  $\sigma_\theta$ . As a result of the different shape of the  $\sigma_\theta$  versus  $\langle \theta \rangle$  relation, the strength of the correlation between the time series of  $e_{j1}$  and  $e_{j2}$  and those of  $\langle \theta \rangle$  and  $\sigma_\theta$  changes with the season (table S4). As noted earlier, the summer season is characterized by sharp changes in  $\langle \theta \rangle$  and  $\sigma_\theta$  due to storm events and high ET rates, while more gradual variations occur in fall and winter. At both sites, the PCs nicely show that  $\theta$  variability results from the superposition of EOF1 with a stable contribution during the year (i.e.,  $e_{j1}$  is positive with limited variability) and EOF2 whose influence depends strongly on seasonality (e.g.,  $e_{j2}$  is positive in wet conditions and negative for dry periods). Sign

changes in  $e_{j2}$  also occur after each storm event, suggesting an important role of EOF2 in the response to precipitation forcing. This is further illustrated through the relative importance of each EOF ( $PV_{1,j}$  and  $PV_{2,j}$ ), which can be linked to the land surface factors exhibiting high correlations to each EOF (table 1). For example, EOF1 is almost always dominant at both sites (i.e.,  $PV_{1,j}$  larger than  $PV_{2,j}$ ), implying that spatial patterns of mesquite cover (SRER) and slope and sand content (JER) dictate soil moisture variability. Time periods when EOF2 increases in importance can be linked to interesting dynamics. For instance, storm events in all seasons lead to increases in  $PV_{2,j}$  followed by recessions during subsequent hiatuses, such that the effects of a mixed combination of land surface factors (SRER) and clay content (JER) on soil moisture variability operate during these periods (table 1). In addition, green-up periods with high NDVI in the summer and prolonged dry periods in the fall and winter seasons also induce a larger role for EOF2, indicating that soil moisture is impacted by vegetation seasonality.

#### 4.3. Physical controls explaining the hysteresis between $\sigma_\theta$ and $\langle \theta \rangle$

The influence of land surface factors on the  $\sigma_\theta$  versus  $\langle \theta \rangle$  relations is analyzed in figure 4 using the proportion of the spatial variance explained by EOF2 relative to the total variance of the first two EOFs ( $PV_{2,j}/(PV_{1,j} + PV_{2,j})$ ). In both semiarid ecosystems, EOF1 generally dominates (blue colors) in the summer season for drier states ( $\langle \theta \rangle$  less than  $0.08 \text{ m}^3 \text{ m}^{-3}$ ), while EOF2 increases in importance (green to red colors) for wetter states ( $\langle \theta \rangle$  greater than  $0.08 \text{ m}^3 \text{ m}^{-3}$ ). Inspection of hysteretic cycles (figure 4 insets and mean values of  $PV_{2,j}/(PV_{1,j} + PV_{2,j})$ )



in table S3) for the summer season reveals that wetting (dry-down) phases are associated with higher (lower) contributions from EOF2, while the redistribution phase exhibits the maximum contribution of EOF2. Furthermore, under these summer conditions, the various physical controls on EOF1 and EOF2 act together to substantially increase  $\sigma_\theta$ , since both  $e_{j1}$  and  $e_{j2}$  are positive, as is clearly seen at JER during storm/interstorm sequences (i.e., high  $\sigma_\theta$  and  $\langle \theta \rangle$ , dark red). In fall and winter, a remarkably different behavior is observed, EOF1 is generally more important at intermediate values of  $\langle \theta \rangle$  and the contributions of EOF2 increase towards the driest and wettest states, in particular at SRER. Based on the hysteretic cycles, the wetting and dry-down phases exhibit the influence of physical factors associated with EOF2 that act to substantially decrease  $\sigma_\theta$ , since  $e_{j2}$  is negative in these cases. At intermediate values of  $\langle \theta \rangle$ , linked to redistribution (SRER) or a transition between wetting and dry-down phases (JER), the dominance of EOF1 indicates that vegetation (soil and terrain) factors at SRER (JER) lead to high  $\sigma_\theta$ . These novel insights from the soil moisture observations are consistent with the numerical experiments of Fatichi *et al* (2015) indicating semiarid vegetation has a major control on  $\sigma_\theta$ , but that its sparseness and seasonality

may lead to conditions where abiotic factors also become important.

## 5. Conclusions

Field-scale spatiotemporal variability of  $\theta$  from dense observation networks in two semiarid ecosystems revealed that the overall shape of the  $\sigma_\theta$  versus  $\langle \theta \rangle$  relation results from the superposition of seasonal patterns and the relation evolves in time according to consecutive hysteretic cycles with shorter (longer) duration in summer (fall/winter). The observed spatiotemporal variability is largely explained by two dominant EOF patterns representing time-stable and seasonally varying contributions which act together to increase (reduce) the field-scale spatial variability in summer (fall/winter). Correlations between EOFs and land surface properties measured at a commensurate high-resolution also indicated that  $\theta$  patterns and hystereses are mainly controlled by vegetation (terrain and soil) factors at the site with higher (lower) vegetation cover. These findings (i) confirm mechanistic interpretations only previously available from modeling studies (e.g., Ivanov *et al* 2010, Fatichi *et al* 2015), and (ii) significantly advance the understanding of  $\theta$  variability and its underlying physical controls at the field scale, which can aid soil moisture retrievals from multiple techniques.

## Acknowledgments

We thank two anonymous reviewers for their comments that helped to improve the quality of the paper. We also thank funding from the US Army Research Office (Grant 56059-EV-PCS), the Jornada Long Term Ecological Research (NSF Grant DEB-1235828) and the Decision Center for a Desert City (NSF Grant SES-1462086). We thank Cody A Anderson, Nicole A Pierini, Adam P Schreiner-McGraw, Ryan C Templeton and Federica Borio for help with data collection and processing. ERV would like to thank the US Fulbright-Garcia Robles and Mexican CONACYT fellowships for support. Datasets are available through at <http://jornada.nmsu.edu/data-catalogs/jornada>.

## References

- Adams D K and Comrie A C 1997 The North American monsoon *Bull. Am. Meteorol. Soc.* **78** 2197–213
- Anderson C A and Vivoni E R 2016 Impact of land surface states within the flux footprint on daytime land-atmosphere coupling in two semiarid ecosystems of the southwestern US *Water Resour. Res.* **52** 4785–800
- Brocca L, Melone F, Moramarco T and Morbidelli R 2010 Spatial-temporal variability of soil moisture and its estimation across scales *Water Resour. Res.* **46** W02516
- Busch F A, Niemann J D and Coleman M 2012 Evaluation of an empirical orthogonal function-based method to downscale soil moisture patterns based on topographical attributes *Hydrol. Process.* **26** 2696–709
- Dillon M E, Collini E A and Ferreir L J 2016 Sensitivity of WRF short-term forecasts to different soil moisture initializations from the GLDAS database over South America in march 2009 *Atmos. Res.* **167** 196–207
- Entekhabi D 1995 Recent advances in land-atmosphere interaction research *Rev. Geophys.* **33** 995–1003
- Entekhabi D *et al* 2010 The soil moisture active passive (SMAP) mission *Proc. IEEE* **98** 704–16
- Famiglietti J S, Ryu D, Berg A A, Rodell M and Jackson T J 2008 Field observations of soil moisture variability across scales *Water Resour. Res.* **44** W01423
- Fatichi S, Katul G G, Ivanov V Y, Pappas C, Paschalis A, Consolo A, Kim J and Burlando P 2015 Abiotic and biotic controls of soil moisture spatiotemporal variability and the occurrence of hysteresis *Water Resour. Res.* **51** 3505–24
- Gómez-Plaza A, Martínez-Mena M, Albaladejo J and Castillo V M 2001 Factors regulating spatial distribution of soil water content in small semiarid catchments *J. Hydrol.* **253** 211–26
- Grayson R B, Western A W, Chiew F H S and Blöschl G 1997 Preferred states in spatial soil moisture patterns: local and nonlocal controls *Water Resour. Res.* **33** 2897–908
- Hannachi A, Jolliffe I T and Stephenson D B 2007 Empirical orthogonal functions and related techniques in atmospheric science: a review *Int. J. Climatol.* **27** 1119–52
- Ivanov V Y, Fatichi S, Jenerette G D, Espeleta J F, Troch P A and Huxman T E 2010 Hysteresis of soil moisture spatial heterogeneity and the ‘homogenizing’ effect of vegetation *Water Resour. Res.* **46** W09521
- Jawson S D and Niemann J D 2007 Spatial patterns from EOF analysis of soil moisture at a large scale and their dependence on soil, land-use, and topographic properties *Adv. Water Resour.* **30** 366–81
- Ji X, Shen C and Riley W J 2015 Temporal evolution of soil moisture statistical fractal and controls by soil texture and regional groundwater flow *Adv. Water Resour.* **86** 155–69
- Korres W, Koyama C N, Fiener P and Schneider K 2010 Analysis of surface soil moisture patterns in agricultural landscapes using empirical orthogonal functions *Hydrol. Earth Syst. Sci.* **14** 751–64
- Lawrence J E and Hornberger G M 2007 Soil moisture variability across climate zones *Geophys. Res. Lett.* **34** L20402
- Li B and Rodell M 2013 Spatial variability and its scale dependency of observed and modeled soil moisture over different climate regions *Hydrol. Earth Syst. Sci.* **17** 1177–88
- Mascaro G and Vivoni E R 2012 Utility of coarse and downscaled soil moisture products at L-band for hydrologic modeling at the catchment scale *Geophys. Res. Lett.* **39** L10403
- Ochsner T E, Cosh M H, Cuenca R H, Dorigo W A, Draper C S, Hagimoto Y, Kerr Y H, Njoku E G, Small E E and Zreda M 2013 State of the art in large-scale soil moisture monitoring *Soil Sci. Soc. Am. J.* **77** 1888–919
- Rosenbaum U, Bogaen H R, Herbst M, Huisman J A, Peterson T J, Weuthen A, Western A W and Vereecken H 2012 Seasonal and event dynamics of spatial soil moisture patterns at the small catchment scale *Water Resour. Res.* **48** W10544
- Seneviratne S I, Corti T, Davin E L, Hirschi M, Jaeger E B, Lehner I, Orlowsky B and Teuling A J 2010 Investigating soil moisture–climate interactions in a changing climate: a review *Earth Sci. Rev.* **99** 125–61
- Tao F, Yokozawa M, Hayashi Y and Lin E 2003 Changes in agricultural water demands and soil moisture in China over the last half-century and their effects on agricultural production *Agric. For. Meteorol.* **118** 251–61
- Van Auken O W 2000 Shrub invasions of North American semiarid grasslands *Annu. Rev. Ecol. Syst.* **31** 197–215
- Vanderlinden K, Vereecken H, Hardelauf H, Herbst M, Martínez G, Cosh M H and Pachepsky Y A 2012 Temporal stability of soil water contents: a review of data and analyses *Vadose Zone J.* **11** 1–20
- Vereecken H, Huisman J A, Pachepsky Y, Montzka C, Van Der Kruk J, Bogaen H, Weihermüller L, Herbst M, Martínez G and Vanderborght J 2014 On the spatio-temporal dynamics of soil moisture at the field scale *J. Hydrol.* **516** 76–96
- Vivoni E R, Rodríguez J C and Watts C J 2010 On the spatiotemporal variability of soil moisture and evapotranspiration in a mountainous basin within the North American monsoon region *Water Resour. Res.* **46** W02509
- Wilks D S 2006 *Statistical Methods in the Atmospheric Sciences* 2nd edn (New York: Academic) p 627
- Yetemen O, Istanbuluoğlu E, Flores-Cervantes J H, Vivoni E R and Bras R L 2015 Ecohydrologic role of solar radiation on landscape evolution *Water Resour. Res.* **51** 1127–57